# Role of twist in modulating the electronic and thermoelectric properties of zigzag graphene nanoribbons

Rouhollah Farghadan *

*Department of Physics, University of Kashan, Kashan 87317-53153, Iran*

(Received 15 June 2024; revised 13 July 2024; accepted 7 August 2024; published 15 August 2024)

We investigate the electronic structure and Seebeck coefficient (SC) of twisted zigzag graphene nanoribbons (TZGNRs) with translational symmetry, considering electron-electron interactions, electric fields, and vacancy defects. Using the mean-field Hubbard model, we find that the semiconducting properties of TZGNRs in the antiferromagnetic ground state are preserved when twisted. However, the energy gap significantly decreases with shorter twist lengths. Unlike GNRs, electric fields, which do not induce spin-polarized features, can reduce the energy gap and SC, and cause a flattening of the band structure around the Fermi energy. The variation in the band energy depends on the twist length and electric field strength. Furthermore, monovacancy defects in TZGNRs induce spin-polarization effects in both the band structure and SC, depending on their spatial position within the nanoribbon structure. These versatile features of TZGNRs indicate their potential in stretchable electronics and thermoelectric applications.

DOI: 10.1103/PhysRevB.110.075132

## I. INTRODUCTION

Mechanical control of electronic properties in two-dimensional honeycomb structures, such as graphene, makes it a promising candidate for stretchable electronics [1–3]. Graphene nanoribbons (GNRs) have garnered significant attention due to their unique edge structures [4] and their ability to exhibit tunable electronic, magnetic, and thermal properties under external forces such as strain [5–10]. Additionally, studies have explored the effects of tensile strain and edge stress on the twisting behavior in GNRs and their implications for band-gap tuning [11,12]. Introducing twists along the axis of nanoribbons has emerged as a promising approach to enhance the functionalities of twisted GNRs (TGNRs) [6,11,13–16]. Moreover, several methods for creating twists and Möbius topologies in GNRs have been described in the literature [17–21], accompanied by studies on the structural stability of these configurations. Twisting effects have been investigated in both zigzag and armchair GNRs. Research has examined the origins of formation and the impact of torsion on the electromechanical properties of helical armchair GNRs, considering both pure edge and edge passivation configurations [8,15]. Density functional theory (DFT) studies have analyzed the variation in band gap and strain energy relative to the twist angle in armchair TGNRs with different nanoribbon widths [14]. Local torsion in armchair GNRs has been investigated, revealing the capability for current switching on/off with the twist angle, both with and without vacancies [13,22]. In zigzag edge GNRs, mechanically twisting the channel region without twisting the electrodes (local torsion) has been shown to predict an ideal spin valve effect [6]. Zigzag GNRs and Möbius strips maintain antiferromagnetic ground states through twisting, with the atomic bonding energy and energy gap changing sensitively with twist angle [23].

Research on ballistic transport demonstrates a sensitive reduction in electron and phonon conductance due to structural changes caused by nanoribbon twisting, with the degree of reduction depending on the twist angle and length [24]. Interestingly, the effect of twisting on the electronic and transport properties of ferromagnetic ZGNRs has been investigated using DFT calculations [25]. The results indicate that local twisting induces a phase transition between the metal and semiconductor. Despite nonmagnetic ZGNRs, the transport properties change sensitively, and spin-resolved transmission coefficients exhibit a spin valve effect. Moreover, twisting causes the spin direction of the two adjacent supercells to become antiparallel [25]. Additionally, applications in stretchable electronics based on twisting graphene, silicene, and black phosphorene nanoribbons demonstrate tunable and nonlinear current-voltage characteristics with negative differential resistance [9,17,26]. Investigations of the thermal properties (both electron and phonon) of twisted GNRs show the potential to control thermal conductance through twisting [7,23,24].

In this paper, we consider a periodic structure of twisted GNRs with zigzag edges and investigate the electronic structure in the presence of electron-electron interactions, electric fields, and vacancy defects using the Hubbard model. Our calculations show that the semiconducting behavior of GNRs in the antiferromagnetic ground state can be preserved by twisting, although significant variations in the energy gap are observed. Specifically, the twist length, electric field, and vacancy defects can all manipulate the energy gap in twisted zigzag GNRs (TZGNRs). Furthermore, we explore the impact of these variations in the electronic structure on the thermoelectric properties, particularly the Seebeck coefficient (SC), with respect to twist length, electric field, and vacancy defects. Notably, a reduction in twist length can increase the energy

*Contact author: rfarghadan@kashanu.ac.ir

 

gap, resulting in up to a 30% increase in the SC. Interestingly, in the presence of vacancies, spin-polarized SC can be achieved.

## II. METHOD

To compute the electronic structure of TZGNRs, we employ the tight-binding approximation along with the mean-field Hubbard model [27,28]. In all calculations, we consider a supercell and compute the tight-binding and Hubbard model for all carbon atoms within the supercell. Additionally, the coherent transport approximation [27] is utilized to determine the SC. The Hamiltonian is formulated as described in Refs. [27,29],

$$\hat{H} = -\sum_{\langle i,j\rangle,\sigma} t'_{ij}\,\hat{c}^{\dagger}_{i\sigma}\hat{c}_{j\sigma} + eE\sum_{i,\sigma} x_i\hat{n}_{i,\sigma} + U\sum_{i}(\hat{n}_{i,\uparrow}\langle\hat{n}_{i,\downarrow}\rangle + \hat{n}_{i,\downarrow}\langle\hat{n}_{i,\uparrow}\rangle - \langle\hat{n}_{i,\uparrow}\rangle\langle\hat{n}_{i,\downarrow}\rangle). \quad (1)$$

The initial term represents the tight-binding Hamiltonian specific to TZGNRs. Here, $c^{\dagger}_{i\sigma}$ and $c_{j\sigma}$ denote the creation and annihilation operators for an electron with spin index $\sigma = \uparrow, \downarrow$ at sites $i$ and $j$, respectively. The hopping parameter $t'_{ij}$ in this context is influenced by the atomic bond length $r$, characterized by an exponential decay relationship as detailed in Ref. [30],

$$t' = t_0 \exp\left[-\beta\left(\frac{r}{r_0} - 1\right)\right]. \quad (2)$$

Here, the parameters $t_0 = 2.7$ eV and $r_0 = 1.42$ Å [30] correspond to the hopping parameter and bond length of unstrained GNR, respectively. The decay rate $\beta = 4.47$, derived from first-principles calculations [31], influences the hopping parameter $t'_{ij}$ in the tight-binding Hamiltonian. The second and third terms characterize the electric field effect and electron-electron interaction within the mean-field approximation, respectively. $E$ is the strength of the electric field and $x_i$ is the position of the carbon atom in the $x$ axis. The on-site Coulomb energy $U$ is assumed to be equal to $t_0$ [32,33]. $ni, \sigma$ is the operator that determines the number of electrons with a specific spin $\sigma$ at site $i$, and $\langle ni, \sigma\rangle$ represents the self-consistently calculated mean value of the number operator. The net magnetization at site $i$ is defined by $\rho_i = (\langle ni, \uparrow\rangle - \langle ni, \downarrow\rangle)\mu_B$, where $\mu_B$ is the Bohr magneton. The transition coefficient in this periodic geometry is determined using mode matching, where Bloch wave functions are adapted across the electrodes and scattering region. It is computed as the sum of all input Bloch waves with positive velocity vectors $\mathbf{k}$. By using the matching Bloch wave function, we calculate the total transmission and spin transmission as follows, $T(\epsilon) = \sum_{\alpha=1}^{M_f}\sum_{i=1}^{N}\psi^{\dagger}_{\alpha i}\psi_{\alpha i}$ and $T_s(\epsilon) = \sum_{\alpha=1}^{M_f}\sum_{i=1}^{N}\psi^{\dagger}_{\alpha i}\sigma_z\psi_{\alpha i}$, where $\psi_{\alpha i}$ is the eigenfunction $\psi_\alpha$ and $\sigma_z$ is the Pauli matrices. Therefore, spin transmission in TZGNRs is calculated by [27] $T_{\uparrow(\downarrow)}(\epsilon) = \frac{T(\epsilon)\pm T_s(\epsilon)}{2}$. The SC is evaluated under an applied temperature gradient in the linear response regime. Defined by the intermediate function, denoted as $L_{n,\sigma}(\mu, T)$ and is calculated by $L_n(\mu, T) = -\frac{1}{h}\int(\epsilon-\mu)^n\frac{\partial f(\epsilon,\mu,T)}{\partial\epsilon}\mathrm{T}(\epsilon)d\epsilon$ [34], where $\triangle T \longrightarrow 0$. The SC is derived as [35]

$$S(\mu, T) = -\frac{1}{|e|T}\frac{L_1(\mu, T)}{L_0(\mu, T)}. \quad (3)$$

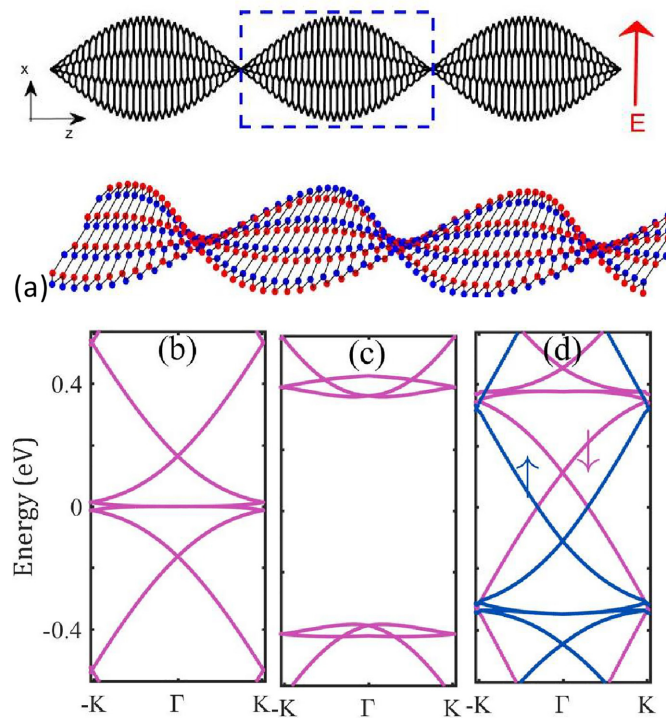


FIG. 1. Representation of twisted zigzag nanoribbons with electronic structures in different magnetic phases. (a) Twisted zigzag nanoribbons with a width of $n = 4$. The dotted rectangular box shows the supercell, which consists of 30 armchair chains and has a length of 7.3 nm. The red arrow and $x$ axis indicate the direction of the electric field. Electronic structure for (b) the nonmagnetic phase, (c) the antiferromagnetic phase, and (d) the ferromagnetic spin configuration.

## III. RESULTS AND DISCUSSION

TZGNRs demonstrate stable structures with magnetic edge states located at the zigzag edges, similar to untwisted GNRs. In this research, we first investigate the chiral structures with various spin configurations. Figure 1(a) depicts the TZGNR with translational symmetry. Each supercell has a length λ, referred to as the twist length. Reducing λ increases the strain in the carbon-carbon bonds. Our calculations in Fig. 1 consider the strength of strain in the regime of low torsion [9], with the minimum twist length for a 4-zigzag chain GNR (4-ZGNR) consisting of 30 armchair chains. The length of the supercell for $L = 30$ is approximately 7.3 nm. We define the torsion coefficient as $\gamma = \frac{W}{\lambda}$, where $W$ is the width of the ribbon. The maximum $\gamma$ in our calculations is approximately 29%. The effect of magnetic configuration on the electronic structure of TZGNR is depicted in Figs. 1(b)–1(d). In the nonmagnetic phase, where the electron-electron interaction is absent, these structures reveal a metallic phase with a highly localized band at the Fermi energy [Fig. 1(b)], attributed to the twisting of nanoribbons. Both the nonmagnetic phase and the ferromagnetic phase exhibit metallic behavior, while the antiferromagnetic phase displays semiconducting behavior with a considerable band gap [Fig. 1(c)]. This band gap minimizes the total energy, making the antiferromagnetic phase the more stable structure. The antiferromagnetic magnetic distribution

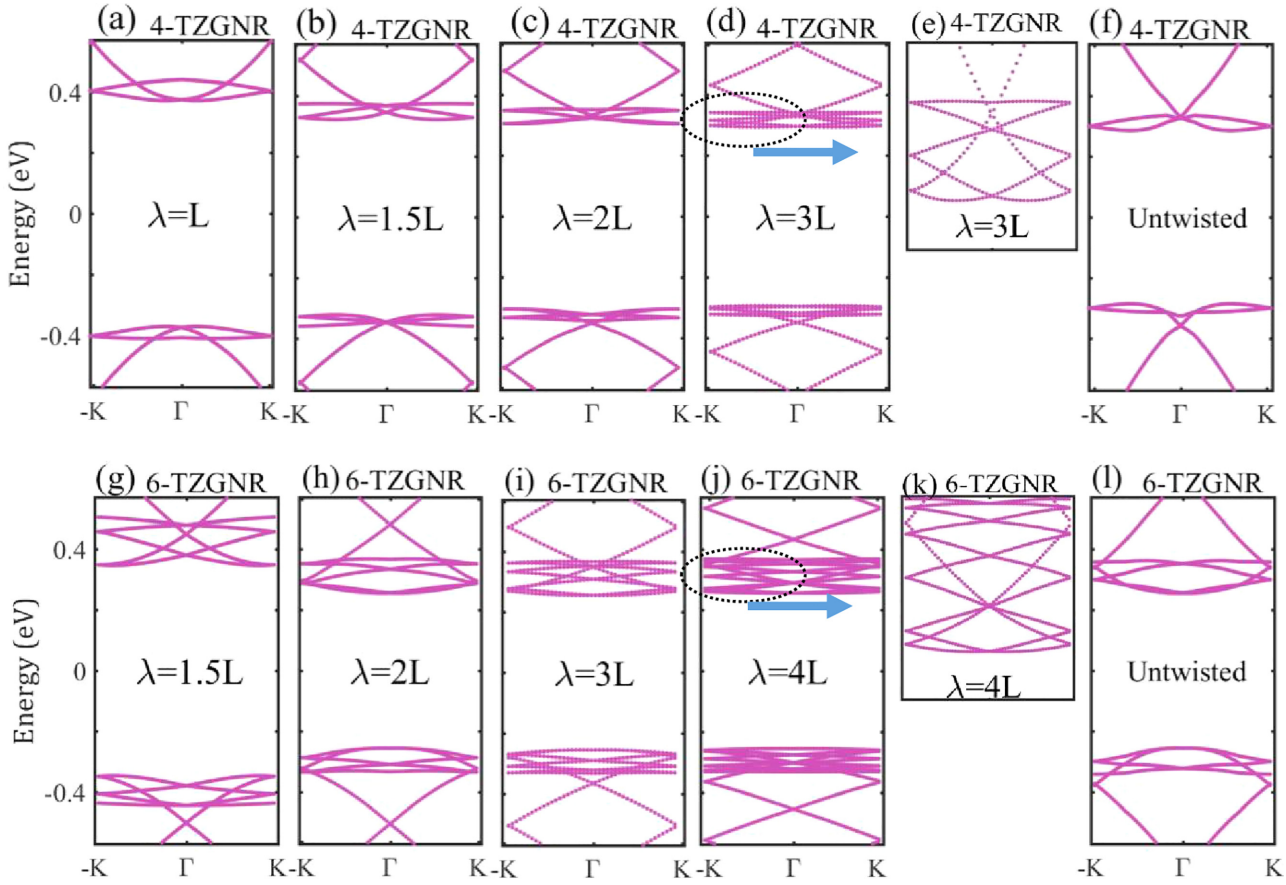


FIG. 2. The variation of the band structure of twisted zigzag graphene nanoribbons with two different widths (4-TZGNR, 6-TZGNR) and varying twist lengths (λ) and $L = 7.3$ nm.

includes different and opposite spin distributions for type-A and type-B atoms in the graphene structure, resulting in different spin orientations at the two zigzag edges. The total magnetization is zero, and there is no spin polarization due to an equal number of two sublattices. In contrast, the ferromagnetic phase exhibits clear spin polarization over a broad energy range [Fig. 1(d)], differing from nontwisted GNRs, which exhibit spin polarization primarily near the Fermi energy.

To characterize the electronic properties of TGNRs, we present the nanoribbon band structure in Fig. 2 for two different widths of TZGNRs. In the antiferromagnetic (AFM) state, the electron spin-up and spin-down bands exhibit complete similarity, with no spin polarization. As the twist length increases, the torsion coefficient decreases, leading to a reduction in the band gap, which approaches the band-gap values of nontwisted nanoribbons. For 4-TZGNR, with $\lambda = L$, $\lambda = 1.5L$, $\lambda = 2L$, $\lambda = 3L$, and untwisted (where $L =$ 30 armchair chains), the energy gaps are 0.75, 0.64, 0.60, 0.58, and 0.57 eV, respectively. Thus, the energy gap increases by approximately 30% for the maximum $\gamma = 29\%$. These variations in the energy gap are also observed for wider TZGNRs. For 6-TZGNR, as λ increases from $1.5L$ to the untwisted state, the energy gap decreases from 0.7 to 0.52 eV. Generally, for various widths of TZGNR in the AFM phase, decreasing the twist length and thus increasing the torsion coefficient results in a significant increase in the energy gap. Increasing the twist length results in a higher number of atoms, which subsequently increases the number of electronic bands. This increase leads to a greater presence of localized states near the Fermi energy [see Figs. 2(e) and 2(k)]. Unlike the AFM phase, the ferromagnetic states display a metallic band structure with spin polarization, a property that persists regardless of changes in the ribbon width.

The electric field has a significant effect on the electronic and magnetic properties of ZGNRs [36,37]. To control these properties, we investigate the influence of the electric field as shown in Figs. 3 and 4. According to Ref. [36], the maximum strength of the electric field for spin splitting in ZGNRs is 1 V/nm. However, in our calculations, we varied the magnitude of the electric field from 0.1 to 2 V/nm. Such an external electric field is experimentally feasible [38].

As seen in Fig. 3, increasing the strength of the electric field does not induce a spin-polarized state in the electronic structure. In an untwisted ZGNR, each edge displays distinct spin-polarized states and encounters varying electric potentials under the influence of the electric field. Consequently, the spin degeneracy between the two spin subbands is disrupted under transverse electric field [see Fig. 3(f)]. However, in twisted ZGNRs, two successive supercells have opposite magnetic configurations at the edges of the nanoribbon. Consequently, both spin states at the edges of the twisted nanoribbon experience similar potentials, preventing the emergence of spin-polarized states. However, at very large

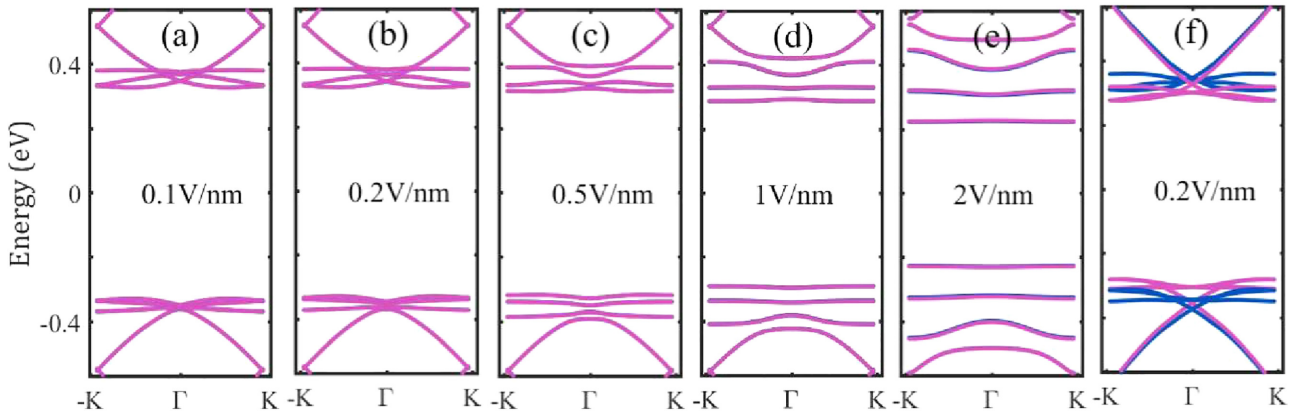


FIG. 3. The effect of an electric field on the electronic structure of twisted and untwisted GNRs. (a)–(e) show 4-TZGNR with a twist length $\lambda = 1.5L$ under various electric field strengths, and (f) depicts an untwisted GNR with a supercell length $\lambda = 1.5L$ and $L = 7.3$ nm.

electric field strengths ($E > 2$ V/nm), a slight spin polarization can be observed. Typically, when $E < 2$ V/nm, the band structure of 4-TZGNR with $\lambda = L$ remains unaffected by changes in electric field strength unlike untwisted GNR [compare Figs. 3(a) and 3(b) with Fig. 3(f)]. However, as the electric field strength increases $E > 3$ V/nm, there is a notable reduction in the energy gap, accompanied by a flattening of the band structure around the Fermi energy. In Figs. 3(c)–3(e), discrete and nearly flat bands emerge near the Fermi energy. These bands become more distinct as the strength of $E$ increases, causing the energy gap to decrease from 0.66 eV at $E = 0.1$ V/nm to 0.46 eV at $E = 0.1$ V/nm. A comparison of Figs. 3(b) and 3(f) shows that $E = 0.2$ V/nm creates a spin-polarized ground state in untwisted GNR, however, this strength of the electric field does not affect the band structure of TZGNR.

Figure 4 illustrates the impact of an electric field on the electronic structure of 4-TZGNRs with different twist lengths, while maintaining a constant electric field strength ($E = 0.2$ V/nm). Interestingly, as the twist length increases, the electric field can more effectively alter the band structure. For instance, for $\lambda = L$ and $2L$, the electric field does not significantly affect the band structure, as observed in Figs. 4(a) and 4(b). However, for larger twist lengths, such as $\lambda = 3L$ and $4L$, the electric field with the same strength ($E = 0.2$ V/nm) creates discrete and flat bands, as observed in Figs. 4(c)–4(e). Generally, the electric field cannot induce spin-polarized states in TZGNRs, and the magnitudes of the field that induce such states in untwisted nanoribbons and reduce the energy gap have no impact on the energy bands of twisted nanoribbons. However, in TZGNRs, an increase in the electric field magnitude beyond the usual for untwisted GNRs results in a notable decrease in the energy gap and a flattening of the band structure. The specific strength of the electric field required to affect the gap energy and band structure in TZGNRs is contingent upon the twist length of the nanoribbons.

To evaluate the thermoelectric performance of the TZGNR, Fig. 5 showcases the SC plotted against the chemical potential. In light of the semiconducting phase, considerable SC are expected in these chiral structures. The symmetrical band structure for electrons and holes results in symmetrical behavior of the SC around the Fermi energy but with differing signs. Furthermore, the sign of the SC indicates the

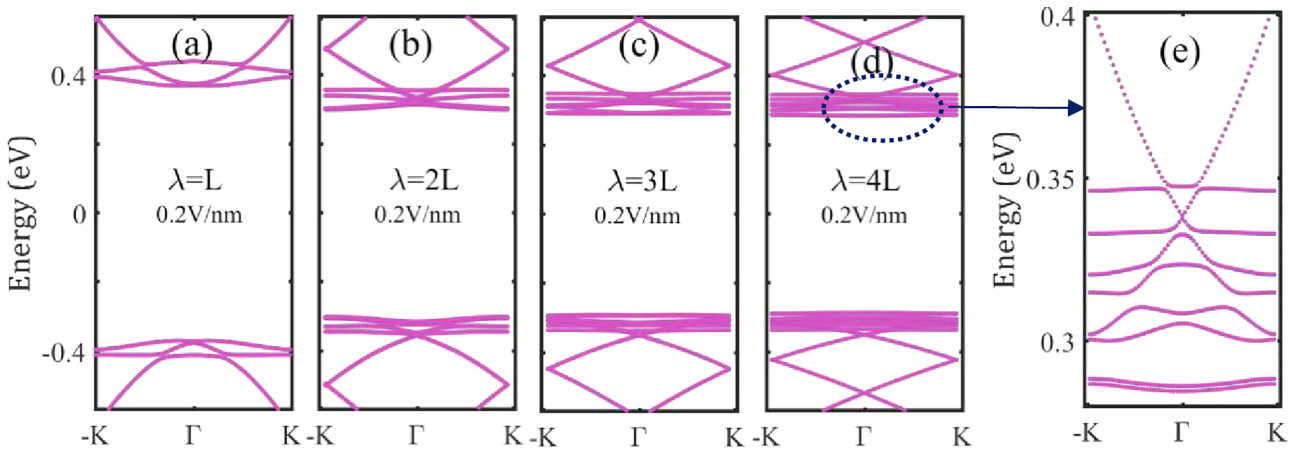


FIG. 4. (a)–(d) illustrate the effect of an electric field on the electronic structure of 4-TZGNRs with different twist lengths and a constant electric field strength ($E = 0.2$ V/nm) and $L = 7.3$ nm. (e) provides an insight into the localized state near the Fermi energy, which becomes a flat band under the electric field effect.

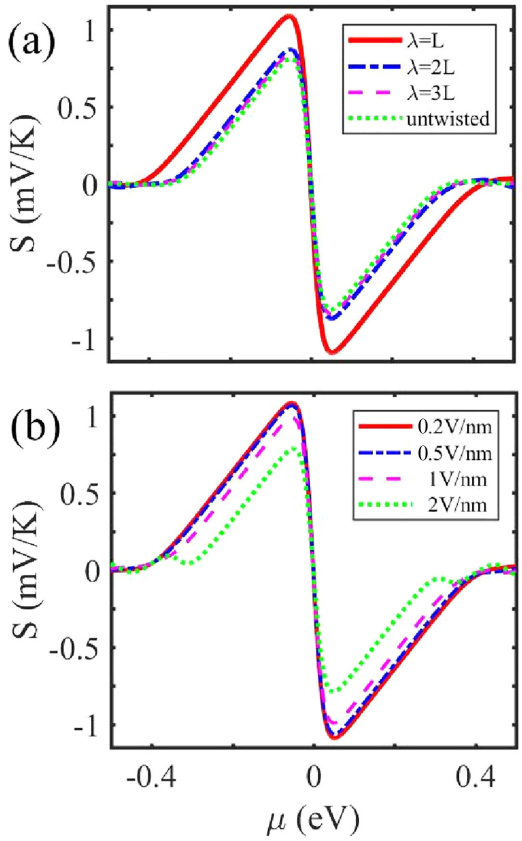


FIG. 5. The impact of twist length and electric field strength on the SC vs chemical potential for 4-TZGNRs is depicted. (a) shows the variation of SC with twist length, while (b) illustrates its variation with electric field strength for $\lambda = 1.5L$.

direction of thermal currents in the channel. These coefficients demonstrate consistency for both up and down spins across all chemical potentials, with a maximum value of about 1 mV/K. As discussed in Fig. 2, twisting the nanoribbons increases the energy gap, which also raises the SC. Figure 5(a) shows that the maximum SC changes from 1.083 mV/K for $\lambda = L$ to 0.811 mV/K for the untwisted nanoribbon. The overall behavior of the SC, particularly around the Fermi energy, remains similar for different twist lengths, but twisting significantly enhances the SC. Generally, decreasing the twist length does not alter the behavior of the SC versus the chemical potential, but it significantly increases the value of SC. In contrast, increasing the electric field strength results in a decrease in the SC. For instance, at $E = 2$ V/nm, the SC drops to 0.780 mV/K [Fig. 5(a)], attributed to the reduction in the energy gap. Due to the potential impact on electronic and thermoelectric properties caused by vacancies in nanoribbons, and considering the strain effects in twisted morphologies that may lead to such defects, we investigate the implications of monovacancy defects in TZGNRs. We propose that these defects occur periodically within all supercells while maintaining translational symmetry. The introduction of vacancy defects disrupts the balance between the two sublattices in the graphene structure, leading to magnetic effects and resulting in a net magnetic moment of $1\mu_B$. We analyze two specific locations for the vacancies: one positioned at the edge and the other at the center of the nanoribbon. As illustrated in Fig. 6(a), an edge defect can completely spin polarize the bands near the Fermi level, thereby creating a bipolar magnetic semiconductor. In contrast, a center defect primarily affects bands located further from the Fermi level and induces relatively less spin polarization, especially notable at the first electron band above the Fermi level where the two spin subbands appear degenerate, as depicted in Fig. 6(b). The disparate behaviors of edge and center defects lead to varying spin-polarized energy bands around the Fermi level. On the other hand, these two different positions of vacancies create distinct band gaps. Consequently, as demonstrated in Figs. 6(c) and 6(d), the SC exhibit distinct values and spin polarizations. Note that for a vacancy at the edge of the nanoribbon [Fig. 6(c)], we observe complete spin polarization at $\mu = 0$, characterized by a clear separation between the two spin components in the band structure [Fig. 6(a)]. In general, taking into account electron interactions within the mean-field Hubbard model and the presence of vacancy defects, TZGNR may exhibit distinctive spin-dependent thermoelectric effects, showing a strong sensitivity to the vacancy's specific location within the nanoribbon.

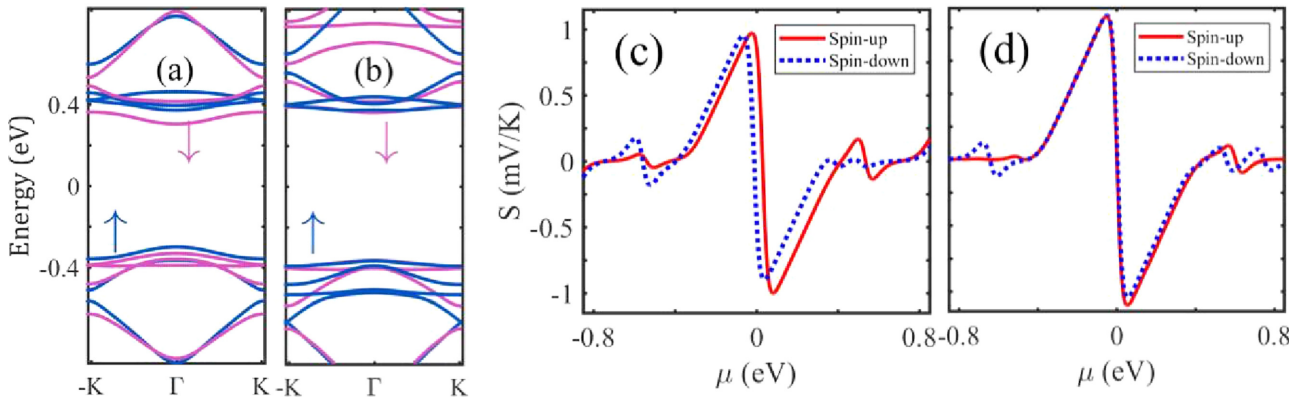


FIG. 6. The impact of vacancy defects on the electronic structure and spin-dependent SC for 4-TZGNRs with $\lambda = L$. (a) and (c) show the effect of edge defects on the band structure and SC, respectively, while (b) and (d) illustrate the variation of the band structure and SC for center defects, respectively.

## IV. CONCLUSION

Due to the edge magnetism inherent in zigzag structures and the intriguing electronic properties introduced by twisting, we have explored how twist length, electric fields, and vacancy defects impact the electronic and thermoelectric characteristics of twisted nanoribbons. Recognizing the importance of caloritronic properties for converting thermal energy into electrical voltages, we have proposed a specialized design for caloritronic components based on these stretchable structures. Our calculations demonstrate that twisted nanoribbons exhibit higher thermoelectric efficiency compared to their untwisted counterparts, primarily due to significant increases in both the energy gap and SC with twist length or torsion coefficient. We have investigated how manipulating the band structure with electric fields can lead to anticipated effects, including the emergence of unpolarized spin features, a decrease in the energy gap, and the flattening of the energy band. Furthermore, our predictions suggest that monovacancy defects induce spin-polarized band structures and spin-dependent Seebeck effects with complete spin polarization, which vary depending on the vacancy's position. In our calculations, we have disregarded the influence of phonons in thermal transfer due to the negligible heat transfer by carbon atoms in graphene nanostructures. Looking ahead, exploring chiral structures of other elements in the fourth group of the periodic table, particularly under spin-orbit interactions and structural defects, holds promise for future research avenues.

## ACKNOWLEDGMENT

This work was financially supported by Iran National Support Foundation (INSF).

[1] J. A. Rogers, T. Someya, and Y. Huang, Materials and mechanics for stretchable electronics, Science **327**, 1603 (2010).

[2] H. Jang, Y. J. Park, X. Chen, T. Das, M.-S. Kim, and J.-H. Ahn, Graphene-based flexible and stretchable electronics, Adv. Mater. **28**, 4184 (2016).

[3] N. Liu, A. Chortos, T. Lei, L. Jin, T. R. Kim, W.-G. Bae, C. Zhu, S. Wang, R. Pfattner, X. Chen *et al.*, Ultratransparent and stretchable graphene electrodes, Sci. Adv. **3**, e1700159 (2017).

[4] A. Saffarzadeh and R. Farghadan, A spin-filter device based on armchair graphene nanoribbons, Appl. Phys. Lett. **98**, 023106 (2011).

[5] O. Hod and G. E. Scuseria, Electromechanical properties of suspended graphene nanoribbons, Nano Lett. **9**, 2619 (2009).

[6] N. Al-Aqtash, H. Li, L. Wang, W.-N. Mei, and R. F. Sabirianov, Electromechanical switching in graphene nanoribbons, Carbon **51**, 102 (2013).

[7] X. Wei, G. Guo, T. Ouyang, and H. Xiao, Tuning thermal conductance in the twisted graphene and gamma graphyne nanoribbons, J. Appl. Phys. **115**, 154313 (2014).

[8] I. Nikiforov, B. Hourahine, Th. Frauenheim, and T. Dumitrica, Formation of helices in graphene nanoribbons under torsion, J. Phys. Chem. Lett. **5**, 4083 (2014).

[9] M. Saiz-Bretín, F. Domínguez-Adame, and A. V. Malyshev, Twisted graphene nanoribbons as nonlinear nanoelectronic devices, Carbon **149**, 587 (2019).

[10] F. Ildarabadi and R. Farghadan, Spin-thermoelectric transport in nonuniform strained zigzag graphene nanoribbons, Phys. Rev. B **103**, 115424 (2021).

[11] D.-B. Zhang and T. Dumitrică, Effective-tensional-strain-driven bandgap modulations in helical graphene nanoribbons, Small **7**, 1023 (2011).

[12] A. Ramasubramaniam, P. Koskinen, O. O. Kit, and V. B. Shenoy, Edge-stress-induced spontaneous twisting of graphene nanoribbons, J. Appl. Phys. **111**, 054302 (2012).

[13] J. Jia, D. Shi, X. Feng, and G. Chen, Electromechanical properties of armchair graphene nanoribbons under local torsion, Carbon **76**, 54 (2014).

[14] A. Sadrzadeh, M. Hua, and B. I. Yakobson, Electronic properties of twisted armchair graphene nanoribbons, Appl. Phys. Lett. **99**, 013102 (2011).

[15] D.-B. Zhang and T. Dumitrică, Role of effective tensile strain in electromechanical response of helical graphene nanoribbons with open and closed armchair edges, Phys. Rev. B **85**, 035445 (2012).

[16] C. Kulkarni, A. K. Mondal, T. K. Das, G. Grinbom, F. Tassinari, M. F. J. Mabesoone, E. W. Meijer, and R. Naaman, Highly efficient and tunable filtering of electrons' spin by supramolecular chirality of nanofiber-based materials, Adv. Mater. **32**, 1904965 (2020).

[17] S. Ma, J. Gu, C. Lin, Z. Luo, Y. Zhu, and J. Wang, Supertwistacene: a helical graphene nanoribbon, J. Am. Chem. Soc. **142**, 16887 (2020).

[18] Y. Segawa, T. Watanabe, K. Yamanoue, M. Kuwayama, K. Watanabe, J. Pirillo, Y. Hijikata, and K. Itami, Synthesis of a Möbius carbon nanobelt, Nat. Synth. **1**, 535 (2022).

[19] T. W. Chamberlain, J. Biskupek, G. A. Rance, A. Chuvilin, T. J. Alexander, E. Bichoutskaia, U. Kaiser, and A. N. Khlobystov, Size, structure, and helical twist of graphene nanoribbons controlled by confinement in carbon nanotubes, ACS Nano **6**, 3943 (2012).

[20] Y. Cao, R. L. Flores, and Y.-Q. Xu, Curling graphene ribbons through thermal annealing, Appl. Phys. Lett. **103**, 183103 (2013).

[21] A. L. Elías, A. R. Botello-Mendez, D. Meneses-Rodriguez, V. J. Gonzalez, D. Ramirez-Gonzalez, L. Ci, E. Munoz-Sandoval, P. M. Ajayan, H. Terrones, and M. Terrones, Longitudinal cutting of pure and doped carbon nanotubes to form graphitic nanoribbons using metal clusters as nanoscalpels, Nano Lett. **10**, 366 (2010).

[22] M. Poliki and S. Haji-Nasiri, Electronic and transport characteristics of vacancy and nitrogen-doped graphene nanoribbon rotational switch, Appl. Phys. A **125**, 658 (2019).

[23] A. V. Savin, E. A. Korznikova, and S. V. Dmitriev, Improving bending rigidity of graphene nanoribbons by twisting, Mech. Mater. **137**, 103123 (2019).

[24] A. Antidormi, M. Royo, and R. Rurali, Electron and phonon transport in twisted graphene nanoribbons, J. Phys. D: Appl. Phys. **50**, 234005 (2017).

[25] H. Li, N. Al-Aqtash, L. Wang, R. Qin, Q. Liu, J. Zheng, W.-N. Mei, R. F. Sabirianov, Z. Gao, and J. Lu, Electromechanical

switch in metallic graphene nanoribbons via twisting, Physica E **44**, 2021 (2012).

[26] S. Carmel, S. Subramanian, R. Rathinam, and A. Bhattacharyya, Twisted monolayer black phosphorus nanoribbbons: Tunable electronic and optical properties, J. Appl. Phys. **127**, 094303 (2020).

[27] M. Shirdel-Havar and R. Farghadan, Spin caloritronics in spin semiconducting armchair graphene nanoribbons, Phys. Rev. B **97**, 235421 (2018).

[28] F. Ildarabadi and R. Farghadan, Carbon atomic chains in a spin thermoelectric device, J. Magn. Magn. Mater. **497**, 165980 (2020).

[29] R. Farghadan and E. Saievar-Iranizad, Spin-polarized edge and magnetoresistance in graphene flake, Solid State Commun. **151**, 1763 (2011).

[30] V. M. Pereira, A. H. Castro Neto, and N. M. R. Peres, Tight-binding approach to uniaxial strain in graphene, Phys. Rev. B **80**, 045401 (2009).

[31] R. Banerjee, V.-H. Nguyen, T. Granzier-Nakajima, L. Pabbi, A. Lherbier, A. R. Binion, J.-C. Charlier, M. Terrones, and E. W. Hudson, Strain modulated superlattices in graphene, Nano Lett. **20**, 3113 (2020).

[32] J. L. Lado and J. Fernández-Rossier, Magnetic edge anisotropy in graphenelike honeycomb crystals, Phys. Rev. Lett. **113**, 027203 (2014).

[33] S. Krompiewski and G. Cuniberti, Edge magnetism impact on electrical conductance and thermoelectric properties of graphenelike nanoribbons, Phys. Rev. B **96**, 155447 (2017).

[34] F. M. Mousavi and R. Farghadan, Electrical control of the spin-seebeck coefficient in graphene nanoribbons with asymmetric zigzag edge extensions, Phys. Chem. Chem. Phys. **24**, 27195 (2022).

[35] S. Esteki and R. Farghadan, Spin thermoelectric properties induced by hydrogen impurities in zigzag graphene nanoribbons, Phys. Chem. Chem. Phys. **26**, 12035 (2024).

[36] Y.-W. Son, M. L. Cohen, and S. G. Louie, Half-metallic graphene nanoribbons, Nature (London) **444**, 347 (2006).

[37] S. Zamani and R. Farghadan, Electric field induced enhancement of photovoltaic effects in graphene nanoribbons, Phys. Rev. B **99**, 235418 (2019).

[38] E. Gruber, R. A. Wilhelm, R. Pétuya, V. Smejkal, R. Kozubek, A. Hierzenberger, B. C. Bayer, I. Aldazabal, A. K. Kazansky, F. Libisch *et al.*, Ultrafast electronic response of graphene to a strong and localized electric field, Nat. Commun. **7**, 13948 (2016).